AIAA JOURNAL
Vol. 32, No. 2, February 1994

Vibratory Characteristics of Cantilevered Rectangular Shallow Shells of Variable Thickness

K. M. Liew* and C. W. Lim†
Nanyang Technological University, 2263 Singapore

In this paper, a comprehensive study on the modeling of vibratory response of variable thickness cantilevered shallow cylindrical shells of rectangular planform is carried out. Through the principle of minimum total energy, the equations of stretching and bending strain energies, kinetic energy, and the associated boundary conditions of the shells are derived. The present model is developed based on the Ritz formulation with the assumption of sets of mathematically complete admissible two-dimensional polynomials to approximate the in-plane and transverse displacement amplitude functions. A basic function is introduced in the approximate method to enforce automatic satisfaction of the kinematic boundary conditions. Sets of comprehensive reasonably accurate vibration frequencies of the shallow shells are presented for wide ranges of aspect ratio, thickness variation ratios, and shallowness ratio. These results, where possible, are verified by comparing with other established experimental and theoretical solutions. Few selected contour plots for the first known mode shapes of these cylindrical shells of variable thickness are included.

I. Introduction

VIBRATION analysis of shell structures has long been a subject of extensive research owing to its practical importance in structural, mechanical, and aerospace applications. Exact solutions to this problem were not sought due to the algebraic complexity of the equations and, therefore, approximate methods must be resorted to for such analysis. There are numerous numerical approaches adopted by researchers, such as the finite element method, the boundary element method, and the method of variational principle of minimum total energy. Of late, the energy method, particularly the Rayleigh-Ritz method, has received intensive attention in the vibration of plates and shells of a variety of specifications, configurations, and boundary conditions. This method is widely acceptable due to its simplicity in implementation and capability to provide satisfactory results.

A relatively complete study by Leissa[1] summarized most of the related work on shell analysis that had been done before 1973. In addition, Lee et al.[2] also presented a numerical study on vibrations of blades with variable thickness and curvature using shallow shell theory. Comparisons of flat plate results with spanwise and chordwise tapers as well as twisted plate and cylindrical shell with chordwise tapers were performed. Olson and Lindberg[3] did an excellent experiment on the uniform and tapered steel fan blades, and the results were verified by numerical methods employing the finite doubly curved triangular elements (FER). The experimental and computational results were further examined by Walker[4] using the doubly curved helicoidal shell elements. Deb Nath[5] conducted an experiment on the natural frequencies of a fully clamped aluminium cylindrical shell, and the outcome was compared by Petyt[6] to some theoretical and computational predictions.

Leissa et al.[7,8] applied the Rayleigh-Ritz minimum total energy method to a number of problems ranging from plates to shells. They employed the simple polynomials to approximate the in-plane and transverse displacement amplitude functions to solve the vibration of cantilevered[7] and rotating blades.[8] Leissa and Ewing[9] further studied the vibration of turbomachinery blades and also made a comparison between the beam and shell theories. Cheung et al.[10] used the finite strip method to investigate the free vibration of circular sectorial plates, the fully clamped cylindrical shell initiated by Deb Nath,[5] the fully clamped conical shells, and the elliptical shells. In the past, relatively few researches, besides Lee et al.,[2] Olson and Lindberg,[3] and Walker[4] have dealt with vibrations of shells with variable thickness. This is the key subject of the present study.

The *pb*-2 Ritz method extensively applied by Liew and his co-workers[11-13] to study the vibration of flat plates is now extended to shell analysis in the present study. It is computationally efficient and, in principle, able to provide numerical results as accurate as required depending on the capability of the computing machine. This approach was used recently by Lim and Liew[14] to study the flexural vibration of a uniform thickness cylindrical shell of rectangular planform subject to a variety of boundary conditions. The unique feature of this method lies in the employment of the admissible *pb*-2 shape function which comprises the product of 1) a complete set of orthogonally generated two-dimensional polynomials and 2) a basic function formed from the product of the geometric equations of boundaries, each raised to an appropriate power corresponding to a free, simply supported or clamped edge, respectively. The in-plane and transverse functions in the present study are expressed in these shape functions. A linear two-dimensional thickness variation function is also introduced to provide for the variations in shell thickness. A similar linear one-dimensional thickness variation function was used earlier by Liew and Lim[13] for the analysis of transverse vibration of symmetric trapezoidal plates of variable thickness.

The main objective of the present study is to investigate the effect of variations in shell thickness on the natural frequencies of flexural vibration of a cantilevered shallow shell, employing and extending the classical Ritz formulation with general *pb*-2 shape functions. The accuracy of the solutions is verified by comparison with some experimental and computational results available from the open literature. Convergence of the numerical results are thoroughly checked. Sets of relatively comprehensive nondimensional vibration frequency parameters for wide ranges of aspect ratio, shallowness ratio, and thickness variation ratios are presented. In addition, some selected contour plots representing the in-plane and transverse mode shapes are included. The effects of certain geometric parameters such as the thickness variation ratios and the shallowness ratio are discussed.

Received June 27, 1992; revision received June 4, 1993; accepted for publication June 4, 1993.

*Director, Dynamics and Vibration Centre, School of Mechanical and Production Engineering.

†Research Assistant, Dynamics and Vibration Centre, School of Mechanical and Production Engineering.

II. Theoretical Formulation

A. Problem Definition

Consider a homogeneous, isotropic, thin shallow cylindrical shell of rectangular planform with varying thickness along the x axis and/or y axis as depicted in Fig. 1. It has a rectangular planform of length a, width b, radius of curvature R_y in the chordwise (i.e., y) direction, thickness $h(x,y)$, and linear thickness variation ratios α_x and α_y in the x and y directions, respectively. The planform is bounded by $-a/2 \le x \le a/2$ and $-b/2 \le y \le b/2$, and the reference thickness h_0 is located at $(-a/2, -b/2)$. Also, $\alpha_x h_0$ is the shell thickness at $(a/2, -b/2)$ whereas $\alpha_y h_0$ is the shell thickness at $(-a/2, b/2)$. The shell is clamped at $x = -a/2$ and is deemed CFFF hereafter. The displacements are resolved into three orthogonal components u, v, and w with respect to the midsurface of the shell with u along the x axis, v tangential to the midsurface, and w normal to it. The problem is to determine the vibration frequencies and mode shapes of this CFFF shallow shell.

B. Formulation of Energy Functional

The total strain energy, $\mathcal{U}$ of a homogeneous, isotropic, thin shallow cylindrical shell with variable thickness is composed of the membrane strain energy $\mathcal{U}_s$, due solely to the stretching effects of the midsurface and the bending strain energy $\mathcal{U}_b$ of the shell, i.e.,

$$\mathcal{U} = \mathcal{U}_s + \mathcal{U}_b \tag{1}$$

and the strain energy components can be expressed as

$$\mathcal{U}_s = 6\int_{-b/2}^{b/2}\int_{-a/2}^{a/2} \frac{D(x,y)}{h^2(x,y)}\left[(\epsilon_x + \epsilon_y)^2 - 2(1-\nu)\left(\epsilon_x\epsilon_y - \frac{1}{4}\gamma_{xy}^2\right)\right] dx\, dy \tag{2}$$

and

$$\mathcal{U}_b = \frac{1}{2}\int_{-b/2}^{b/2}\int_{-a/2}^{a/2} D(x,y)\left\{(\Delta w)^2 - 2(1-\nu)\left[\frac{\partial^2 w}{\partial x^2}\frac{\partial^2 w}{\partial y^2} - \left(\frac{\partial^2 w}{\partial x \partial y}\right)^2\right]\right\} dx\, dy \tag{3}$$

where the flexural rigidity $D(x,y) = Eh^3(x,y)/12(1-\nu^2)$, E is Young's modulus, ν is Poisson's ratio, and Δ is the Laplacian operator defined as $(\partial^2/\partial x^2 + \partial^2/\partial y^2)$. The strains of the membrane can be expressed in terms of the displacements as

$$\epsilon_x = \frac{\partial u}{\partial x} \tag{4a}$$

$$\epsilon_y = \frac{\partial v}{\partial y} + \frac{w}{R_y} \tag{4b}$$

$$\gamma_{xy} = \frac{\partial v}{\partial x} + \frac{\partial u}{\partial y} \tag{4c}$$

The kinetic energy is given by

$$\mathcal{T} = \frac{\rho}{2}\int_{-b/2}^{b/2}\int_{-a/2}^{a/2} h(x,y)\left[\left(\frac{\partial u}{\partial t}\right)^2 + \left(\frac{\partial v}{\partial t}\right)^2 + \left(\frac{\partial w}{\partial t}\right)^2\right] dx\, dy \tag{5}$$

where ρ is the mass density per unit volume. The linearly varying shell thickness can be expressed as

$$h(x,y) = h_0\, g(x,y) \tag{6}$$

where $g(x,y)$ is the thickness variation function to be given in due course. The flexural rigidity of the shell is given by

$$D(x,y) = D_0\, g^3(x,y) \tag{7}$$

where $D_0 = Eh_0^3/12(1-\nu^2)$ is the reference flexural rigidity.

Assuming the free vibration amplitude to be small, the displacement functions then take the following forms:

$$u(x,y,t) = U(x,y)\sin\omega t \tag{8a}$$

$$v(x,y,t) = V(x,y)\sin\omega t \tag{8b}$$

$$w(x,y,t) = W(x,y)\sin\omega t \tag{8c}$$

where ω denotes the angular frequency of vibration. Using Eqs. (4a-4c) and (8a-8c), the strain energy and kinetic energy components, Eqs. (2), (3), and (5), can be simplified to the following expressions:

$$(\mathcal{U}_s)_{\max} = \frac{6D_0}{h_0^2}\int_{-b/2}^{b/2}\int_{-a/2}^{a/2} g(x,y)\left\{\left(\frac{\partial U}{\partial x}\right)^2 + \left(\frac{\partial V}{\partial y}\right)^2 + \left(\frac{W}{R_y}\right)^2 + 2\frac{W}{R_y}\frac{\partial V}{\partial y} + 2\nu\frac{\partial U}{\partial x}\left(\frac{\partial V}{\partial y} + \frac{W}{R_y}\right) + \frac{1-\nu}{2}\left[\left(\frac{\partial V}{\partial x}\right)^2 + 2\frac{\partial V}{\partial x}\frac{\partial U}{\partial y} + \left(\frac{\partial U}{\partial y}\right)^2\right]\right\} dx\, dy \tag{9a}$$

$$(\mathcal{U}_b)_{\max} = \frac{D_0}{2}\int_{-b/2}^{b/2}\int_{-a/2}^{a/2} g^3(x,y)\left\{(\Delta W)^2 - 2(1-\nu)\left[\frac{\partial^2 W}{\partial x^2}\frac{\partial^2 W}{\partial y^2} - \left(\frac{\partial^2 W}{\partial x \partial y}\right)^2\right]\right\} dx\, dy \tag{9b}$$

$$\mathcal{T}_{\max} = \frac{\rho h_0 \omega^2}{2}\int_{-b/2}^{b/2}\int_{-a/2}^{a/2} g(x,y)(U^2 + V^2 + W^2)\, dx\, dy \tag{9c}$$

where $(\mathcal{U}_s)_{\max}$, $(\mathcal{U}_b)_{\max}$, and $\mathcal{T}_{\max}$ are the maximum stretching strain energy, maximum bending strain energy, and maximum kinetic energy in a vibratory circle, respectively. Let $\mathcal{F}_{\max}$ be the total energy functional given by

$$\mathcal{F}_{\max} = \mathcal{U}_{\max} - \mathcal{T}_{\max} \tag{10}$$

where $\mathcal{U}_{\max}$ is the sum of Eqs. (9a and 9b).

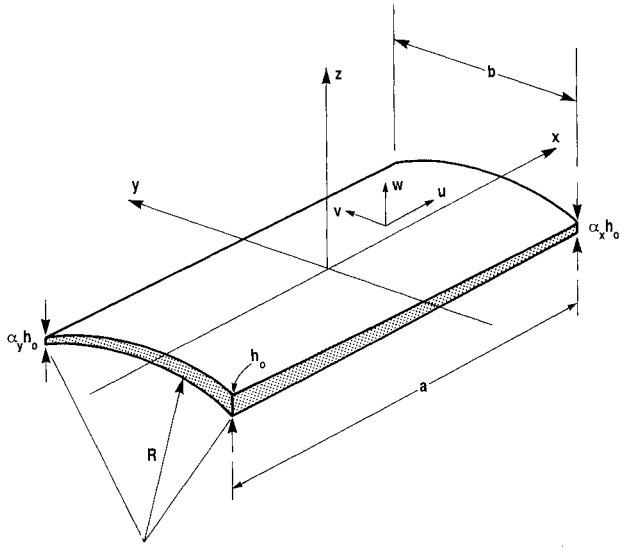

Fig. 1 Geometry of the cylindrical shell with x- and y-varying thickness.

C. Formulation of Governing Eigenvalue Equation

A nondimensional coordinate system is introduced, for simplicity and generality, as follows:

$$\xi = x/a \tag{11a}$$

$$\eta = y/b \tag{11b}$$

where a and b are the length and width of the shell planform as shown in Fig. 1. Therefore, the nondimensional thickness variation function can be expressed as

$$g(\xi,\eta) = 1 - (1-\alpha_x)(\xi + \tfrac{1}{2}) - (1-\alpha_y)(\eta + \tfrac{1}{2})$$

$$g(\xi,\eta) \geq 0 \tag{12}$$

Moreover, the displacement amplitude functions $U(\xi,\eta)$, $V(\xi,\eta)$, and $W(\xi,\eta)$ can be approximated by two-dimensional polynomials of the forms

$$U(\xi,\eta) = \sum_{i=1}^{m} C_{ui}\phi_{ui}(\xi,\eta) \tag{13a}$$

$$V(\xi,\eta) = \sum_{i=1}^{m} C_{vi}\phi_{vi}(\xi,\eta) \tag{13b}$$

$$W(\xi,\eta) = \sum_{i=1}^{m} C_{wi}\phi_{wi}(\xi,\eta) \tag{13c}$$

where C_{ui}, C_{vi}, and C_{wi} are the unknown coefficients and ϕ_{ui}, ϕ_{vi}, and ϕ_{wi} are the corresponding pb-2 shape functions to be discussed in due course.

The geometric boundary conditions for the clamped edge at $\xi = -0.5$ are

$$U|_{\xi=-0.5} = 0 \tag{14a}$$

$$V|_{\xi=-0.5} = 0 \tag{14b}$$

$$W|_{\xi=-0.5} = 0 \tag{14c}$$

and

$$\left.\frac{\partial W}{\partial \xi}\right|_{\xi=-0.5} = 0 \tag{14d}$$

The total energy functional in Eq. (10) is then minimized with respect to the coefficients according to the Ritz principle,

$$\frac{\partial \mathfrak{F}_{\max}}{\partial C_{ui}} = 0 \tag{15a}$$

$$\frac{\partial \mathfrak{F}_{\max}}{\partial C_{vi}} = 0 \tag{15b}$$

$$\frac{\partial \mathfrak{F}_{\max}}{\partial C_{wi}} = 0 \tag{15c}$$

Substituting Eqs. (13a–13c) into the equivalent maximum energy forms in Eqs. (9a–9c) results in

$$\frac{\partial(\mathfrak{U}_s)_{\max}}{\partial C_{ui}} = \frac{12abD_0}{h_0^2}\left[\frac{1}{a^2}\sum_{j=1}^{m} C_{uj}\,\mathcal{G}_{uiuj}^{1010} + \nu\left(\frac{1}{ab}\sum_{j=1}^{m} C_{vj}\,\mathcal{G}_{uivj}^{1001} + \frac{1}{aR}\sum_{j=1}^{m} C_{wj}\,\mathcal{G}_{uiwj}^{1000}\right) + \frac{1-\nu}{2}\left(\frac{1}{b^2}\sum_{j=1}^{m} C_{uj}\,\mathcal{G}_{uiuj}^{0101} + \frac{1}{ab}\sum_{j=1}^{m} C_{vj}\,\mathcal{G}_{uivj}^{0110}\right)\right] \tag{16a}$$

$$\frac{\partial(\mathfrak{U}_s)_{\max}}{\partial C_{vi}} = \frac{12abD_0}{h_0^2}\left[\frac{\nu}{ab}\sum_{j=1}^{m} C_{uj}\,\mathcal{G}_{viuj}^{0110} + \frac{1}{b^2}\sum_{j=1}^{m} C_{vj}\,\mathcal{G}_{vivj}^{0101} + \frac{1}{bR}\sum_{j=1}^{m} C_{wj}\,\mathcal{G}_{viwj}^{0100} + \frac{1-\nu}{2}\left(\frac{1}{ab}\sum_{j=1}^{m} C_{uj}\,\mathcal{G}_{viuj}^{1001} + \frac{1}{a^2}\sum_{j=1}^{m} C_{vj}\,\mathcal{G}_{vivj}^{1010}\right)\right] \tag{16b}$$

$$\frac{\partial(\mathfrak{U}_s)_{\max}}{\partial C_{wi}} = \frac{12abD_0}{h_0^2}\left[\frac{\nu}{aR}\sum_{j=1}^{m} C_{uj}\,\mathcal{G}_{wiuj}^{0010} + \frac{1}{bR}\sum_{j=1}^{m} C_{vj}\,\mathcal{G}_{wivj}^{0001} + \frac{1}{R^2}\sum_{j=1}^{m} C_{wj}\,\mathcal{G}_{wiwj}^{0000}\right] \tag{16c}$$

$$\frac{\partial(\mathfrak{U}_b)_{\max}}{\partial C_{ui}} = 0 \tag{17a}$$

$$\frac{\partial(\mathfrak{U}_b)_{\max}}{\partial C_{vi}} = 0 \tag{17b}$$

$$\frac{\partial(\mathfrak{U}_b)_{\max}}{\partial C_{wi}} = \frac{D_0}{ab}\left[\left(\frac{b}{a}\right)^2\left(\sum_{j=1}^{m} C_{wj}\,\mathcal{G}_{wiwj}^{2020}\right) + \left(\frac{a}{b}\right)^2\left(\sum_{j=1}^{m} C_{wj}\,\mathcal{G}_{wiwj}^{0202}\right) + \nu\left(\sum_{j=1}^{m} C_{wj}\,\mathcal{G}_{wiwj}^{0220} + \sum_{j=1}^{m} C_{wj}\,\mathcal{G}_{wiwj}^{2002}\right) + 2(1-\nu)\sum_{j=1}^{m} C_{wj}\,\mathcal{G}_{wiwj}^{1111}\right] \tag{17c}$$

and

$$\frac{\partial \mathfrak{I}_{\max}}{\partial C_{ui}} = \rho h_0\omega^2 ab\sum_{j=1}^{m} C_{uj}\,\mathcal{G}_{uiuj}^{0000} \tag{18a}$$

$$\frac{\partial \mathfrak{I}_{\max}}{\partial C_{vi}} = \rho h_0\omega^2 ab\sum_{j=1}^{m} C_{vj}\,\mathcal{G}_{vivj}^{0000} \tag{18b}$$

$$\frac{\partial \mathfrak{I}_{\max}}{\partial C_{wi}} = \rho h_0\omega^2 ab\sum_{j=1}^{m} C_{wj}\,\mathcal{G}_{wiwj}^{0000} \tag{18c}$$

where

$$\mathcal{G}_{uiuj}^{defg} = \int_{-0.5}^{0.5}\int_{-0.5}^{0.5} g(\xi,\eta)\frac{\partial^{d+e}\phi_{ui}(\xi,\eta)}{\partial\xi^d\partial\eta^e}\frac{\partial^{f+g}\phi_{uj}(\xi,\eta)}{\partial\xi^f\partial\eta^g}\,d\xi\,d\eta \tag{19a}$$

$$\mathcal{G}_{uivj}^{defg} = \int_{-0.5}^{0.5}\int_{-0.5}^{0.5} g(\xi,\eta)\frac{\partial^{d+e}\phi_{ui}(\xi,\eta)}{\partial\xi^d\partial\eta^e}\frac{\partial^{f+g}\phi_{vj}(\xi,\eta)}{\partial\xi^f\partial\eta^g}\,d\xi\,d\eta \tag{19b}$$

$$\mathcal{G}_{uiwj}^{defg} = \int_{-0.5}^{0.5}\int_{-0.5}^{0.5} g(\xi,\eta)\frac{\partial^{d+e}\phi_{ui}(\xi,\eta)}{\partial\xi^d\partial\eta^e}\frac{\partial^{f+g}\phi_{wj}(\xi,\eta)}{\partial\xi^f\partial\eta^g}\,d\xi\,d\eta \tag{19c}$$

$$\mathcal{G}_{vivj}^{defg} = \int_{-0.5}^{0.5}\int_{-0.5}^{0.5} g(\xi,\eta)\frac{\partial^{d+e}\phi_{vi}(\xi,\eta)}{\partial\xi^d\partial\eta^e}\frac{\partial^{f+g}\phi_{vj}(\xi,\eta)}{\partial\xi^f\partial\eta^g}\,d\xi\,d\eta \tag{19d}$$

$$\mathcal{G}_{viwj}^{defg} = \int_{-0.5}^{0.5}\int_{-0.5}^{0.5} g(\xi,\eta)\frac{\partial^{d+e}\phi_{vi}(\xi,\eta)}{\partial\xi^d\partial\eta^e}\frac{\partial^{f+g}\phi_{wj}(\xi,\eta)}{\partial\xi^f\partial\eta^g}\,d\xi\,d\eta \tag{19e}$$

$$\mathcal{G}_{wiwj}^{defg} = \int_{-0.5}^{0.5}\int_{-0.5}^{0.5} g(\xi,\eta)\frac{\partial^{d+e}\phi_{wi}(\xi,\eta)}{\partial\xi^d\partial\eta^e}\frac{\partial^{f+g}\phi_{wj}(\xi,\eta)}{\partial\xi^f\partial\eta^g}\,d\xi\,d\eta \tag{19f}$$

$$\mathcal{J}_{wiwj}^{defg} = \int_{-0.5}^{0.5}\int_{-0.5}^{0.5} g^3(\xi,\eta)\frac{\partial^{d+e}\phi_{wi}(\xi,\eta)}{\partial\xi^d\partial\eta^e}\frac{\partial^{f+g}\phi_{wj}(\xi,\eta)}{\partial\xi^f\partial\eta^g}\,d\xi\,d\eta \tag{19g}$$

and $i, j = 1, 2, \ldots, m$. The double integrations are symmetric and, in general,

$$\mathcal{G}_{\alpha i\beta j}^{defg} = \mathcal{G}_{\beta j\alpha i}^{fgde} \tag{20a}$$

$$\mathcal{J}_{\alpha i\beta j}^{defg} = \mathcal{J}_{\beta j\alpha i}^{fgde} \tag{20b}$$

The minimization of the energy functional as given by Eqs. (15a–15c) leads to the governing eigenvalue equation as follows:

$$\left(12\begin{bmatrix}[\mathfrak{U}_{uu}] & [\mathfrak{U}_{uv}] & [\mathfrak{U}_{uw}]\\ & [\mathfrak{U}_{vv}] & [\mathfrak{U}_{vw}]\\ \text{sym} & & [\mathfrak{U}_{ww}]\end{bmatrix} - \lambda^2\begin{bmatrix}[\mathfrak{I}_{uu}] & [0] & [0]\\ & [\mathfrak{I}_{vv}] & [0]\\ \text{sym} & & [\mathfrak{I}_{ww}]\end{bmatrix}\right)\begin{Bmatrix}\{C_{uj}\}\\ \{C_{vj}\}\\ \{C_{wj}\}\end{Bmatrix} = \begin{Bmatrix}\{0\}\\ \{0\}\\ \{0\}\end{Bmatrix} \tag{21}$$

where

$$\mathfrak{U}_{uuij} = \left(\frac{b}{h_0}\right)^2 \mathcal{G}_{uiuj}^{1010} + \left(\frac{1-\nu}{2}\right)\left(\frac{a}{h_0}\right)^2 \mathcal{G}_{uiuj}^{0101} \tag{22a}$$

$$\mathfrak{U}_{uvij} = \nu\left(\frac{a}{h_0}\right)\left(\frac{b}{h_0}\right)\mathcal{G}_{uivj}^{1001} + \left(\frac{1-\nu}{2}\right)\left(\frac{a}{h_0}\right)\left(\frac{b}{h_0}\right)\mathcal{G}_{uivj}^{0110} \tag{22b}$$

$$\mathfrak{U}_{uwij} = \nu\left(\frac{a}{R}\right)\left(\frac{b}{h_0}\right)^2 \mathcal{G}_{uiwj}^{1000} \tag{22c}$$

$$\mathfrak{U}_{vvij} = \left(\frac{a}{h_0}\right)^2 \mathcal{G}_{vivj}^{0101} + \left(\frac{1-\nu}{2}\right)\left(\frac{b}{h_0}\right)^2 \mathcal{G}_{vivj}^{1010} \tag{22d}$$

$$\mathfrak{U}_{vwij} = \left(\frac{a}{h_0}\right)^2\left(\frac{b}{R}\right)\mathcal{G}_{viwj}^{0100} \tag{22e}$$

$$\mathfrak{U}_{wwij} = \left(\frac{a}{h_0}\right)^2\left(\frac{b}{R}\right)^2 \mathcal{G}_{wiwj}^{0000} + \frac{1}{12}\left[\left(\frac{b}{a}\right)^2 \mathcal{G}_{wiwj}^{2020} + \left(\frac{a}{b}\right)^2 \mathcal{G}_{wiwj}^{0202}\right.$$
$$\left. + \nu\left(\mathcal{G}_{wiwj}^{0220} + \mathcal{G}_{wiwj}^{2002}\right) + 2(1-\nu)\mathcal{G}_{wiwj}^{1111}\right. \tag{22f}$$

$$\mathfrak{I}_{uuij} = \mathcal{G}_{uiuj}^{0000} \tag{22g}$$

$$\mathfrak{I}_{vvij} = \mathcal{G}_{vivj}^{0000} \tag{22h}$$

$$\mathfrak{I}_{wwij} = \mathcal{G}_{wiwj}^{0000} \tag{22i}$$

$$\lambda = \omega ab\sqrt{\frac{\rho h_0}{D_0}} \tag{22j}$$

where $i, j = 1, 2, \ldots, m$, and m depends on the degree set of polynomials which will be discussed in the next section. The nondimensional frequency parameter λ appears as the eigenvalue in Eq. (21).

D. *pb*-2 Shape Functions

The *pb*-2 shape functions for U, V, and W are ϕ_{ui}, ϕ_{vi}, and ϕ_{wi}, respectively. These shape functions are fundamentally sets of kinematically oriented admissible functions which are composed of the product of terms (indicated by i) of a mathematically complete two-dimensional orthogonally generated polynomials (p-2) and a basic function (b), i.e.,

$$\phi_{\alpha i}(\xi,\eta) = f_i(\xi,\eta)\phi_{\alpha 1} - \sum_{j=1}^{i-1} \Xi_{\alpha ij}\phi_{\alpha j} \tag{23}$$

where

$$\Xi_{\alpha ij} = \left[\int\int_A f_i(\xi,\eta)\phi_{\alpha 1}\phi_{\alpha j}\, d\xi\, d\eta\right]/\left[\int\int_A \phi_{\alpha j}^2\, d\xi\, d\eta\right]$$
$$\alpha = u,\ v \text{ and } w \tag{24}$$

$\sum_{i=1}^{m} f_i(\xi,\eta)$ forms a complete set of p-2 functions. On the other hand, $\phi_{\alpha 1}$ is the basic function defined by the product of the equations of the continuous piecewise boundary geometric expressions each of which is raised to a basic power depending on the types of boundary constraints imposed on the shell, i.e.,

$$\phi_{\alpha 1}(\xi,\eta) = \prod_{i=1}^{n_e}[\Gamma_i(\xi,\eta)]^{\gamma_{\alpha i}} \tag{25}$$

and $\alpha = u$, v, and w where n_e is the number of supporting edges, Γ_i is the boundary expression of the ith supporting edge, and $\gamma_{\alpha i}$, ($\alpha = u$, v, and w) are the basic powers. The powers for the transverse boundary conditions ($\alpha = w$) are 0, 1, or 2 corresponding to a free, simply supported, or clamped edge. However, for the in-plane boundary conditions ($\alpha = u$ and v), the power is 0 for a completely free edge and 1 for either a simply supported or clamped edge. For a cantilevered shallow shell, the corresponding basic functions are

$$\phi_{u1}(\xi) = (\xi + 0.5) \tag{26a}$$

$$\phi_{v1}(\xi) = (\xi + 0.5) \tag{26b}$$

$$\phi_{w1}(\xi) = (\xi + 0.5)^2 \tag{26c}$$

The mathematically complete two-dimensional polynomial $\sum_{i=1}^{m} f_i(\xi,\eta)$ can be expressed as

$$\sum_{i=1}^{m} f_i(\xi,\eta) = \sum_{q=0}^{p}\sum_{i=0}^{q} \xi^{q-i}\eta^i \tag{27}$$

with m and p related by

$$m = [(p+1)(p+2)]/2 \tag{28}$$

where p is the degree of the complete set of two-dimensional polynomials employed.

III. Numerical Examples and Discussion

The *pb*-2 Ritz approach is applied to model the vibratory behavior of a cantilevered (CFFF) shallow cylindrical shell of variable thickness. In the current paper, a clamped edge is given the notation C and a free edge is denoted by F. The clamped edge is at $x = -a/2$. The convergence of the approximate method to an upper-bound value is numerically verified, and a comparison study with experimental as well as finite element results available from the open literature is carried out.

A. Convergence Study

Two cases are selected to demonstrate the convergence of the eigenvalues (frequency parameters) of Eq. (21), one with x-varying thickness and the other with y-varying thickness (see Table 1). The aspect ratio a/b investigated is 1.0, whereas the degree of the complete set of polynomials p ranges from 13 to 18. The corresponding determinants for the eigenequation (21) can be determined by Eq.(28) which ranges from 315 to 570. The values of x-thickness variation ratio α_x examined are 0.0 (a sharp edge at $x = a/2$) and 1.0 (uniform thickness); and for the y-thickness variation ratio α_y, the values are 0.0 (a sharp edge at $y = b/2$) and 2.0.

It is obvious from Table 1 that the convergence of eigenvalue to an upper-bound value is ensured as the degree of polynomial increases. For $p = 18$, the eigenvalues are generally accurate up to four significant figures except for a few higher modes (mode 7 and mode 8). On the contrary, the lower modes (mode 1 and mode 2) are convergent to five significant figures. For generality, $p = 18$ is chosen for all of the computations and five significant figures for the eigenvalues are displayed throughout the present paper, bearing in mind that some higher modes may converge up to three or four significant figures.

Lim and Liew[14] have shown that a uniform thickness shallow shell with more boundary constraints (more edges are simply supported or clamped) has faster rate of eigenvalue convergence. For example, $p = 15$ is sufficient for eigenvalues with five convergent significant figures for a SSSS (fully simply supported) shallow shell of uniform thickness. It has also been shown that for a CFFF shallow shell, $p = 15$ is able to give eigenvalues as accurate as four significant figures. To achieve the same order of accuracy for the present case, $p = 18$ must be set. Consequently, shallow shells with varying thickness have relatively slower rate of convergence of eigenvalues.

B. Comparison Study

Olson and Lindberg[3] had conducted an experiment on the flexural vibration of a tapered steel fan blade. The fan blade has uniform thickness in the x direction ($\alpha_x = 1.0$) and y-thickness variation ratio $\alpha_y = 3.4375$. Olson and Lindberg[3] had also presented the numerical results obtained using the doubly curved finite elements (FET). Similar calculations had also been performed by Walker[4] using the doubly curved helicoidal elements (FEH). The results of the experiment for the aforementioned finite element methods are reproduced in

Table 1 Convergence study of frequency parameters $\lambda = \omega ab\sqrt{\rho h_0/D_0}$ with increases in degree set of complete polynomials for the CFFF shallow shells

$\nu = 0.3$, $b/h_0 = 100$, $b/R_y = 0.5$, $a/b = 1.0$									
		Mode sequence number							
α_x	p	1	2	3	4	5	6	7	8
		x-varying thickness, $\alpha_y = 1.0$							
	13	13.278	13.426	25.106	28.206	34.996	38.264	42.222	42.418
	14	13.277	13.425	25.079	28.168	34.934	38.260	42.072	42.414
0.0	15	13.275	13.424	25.055	28.163	34.878	38.259	41.938	42.411
	16	13.275	13.424	25.047	28.145	34.856	38.256	41.893	42.408
	17	13.274	13.423	25.046	28.125	34.854	38.254	41.886	42.405
	18	13.274	13.423	25.044	28.117	34.848	38.253	41.873	42.403
	13	10.591	16.984	30.643	42.218	47.676	65.440	89.740	89.955
	14	10.590	16.982	30.642	42.214	47.672	65.440	89.734	89.950
1.0	15	10.589	16.981	30.641	42.211	47.668	65.439	89.727	89.947
	16	10.589	16.980	30.641	42.208	47.666	65.439	89.723	89.944
	17	10.589	16.979	30.640	42.206	47.663	65.439	89.718	89.942
	18	10.588	16.978	30.640	42.205	47.662	65.439	89.715	89.939
		y-varying thickness, $\alpha_x = 1.0$							
	13	8.1433	12.218	19.459	20.435	28.736	29.563	36.779	36.806
	14	8.1427	12.217	19.458	20.433	28.727	29.562	36.482	36.789
0.0	15	8.1422	12.217	19.457	20.431	28.723	29.561	36.400	36.786
	16	8.1418	12.216	19.457	20.430	28.720	29.560	36.381	36.784
	17	8.1415	12.216	19.457	20.429	28.718	29.560	36.376	36.783
	18	8.1412	12.216	19.456	20.429	28.717	29.560	36.373	36.781
	13	14.642	18.780	41.761	51.684	67.481	95.596	100.26	105.87
	14	14.641	18.778	41.760	51.680	67.476	95.595	100.25	105.86
2.0	15	14.640	18.777	41.759	51.677	67.471	95.594	100.25	105.86
	16	14.639	18.776	41.759	51.674	67.467	95.594	100.25	105.85
	17	14.639	18.775	41.758	51.672	67.464	95.594	100.24	105.85
	18	14.638	18.774	41.758	51.670	67.462	95.593	100.24	105.85

Table 2 Comparison of frequencies (Hz) of experimental and computational solutions for the CFFF tapered fan blade; values in parentheses indicate the error percentages with reference to the experimental data

$E = 200$ GPa, $\rho = 7860$ kg/m^3, $\nu = 0.3$, $R_y = 30.0$ in., $h_0 = 0.048$ in., $a = b = 12.0$ in., $\alpha_x = 1.0$, $\alpha_y = 3.4375$												
	Mode sequence number											
References	1	2	3	4	5	6	7	8	9	10	11	12
Experiment[2]	76.4	108	202	253	364	426	465	572	677	592	787	808
FET[2]	78.855	114.10	211.55	258.09	370.60	452.32	480.52	581.32	690.11	755.03	805.75	844.88
	(3.2)	(5.6)	(4.7)	(2.0)	(1.8)	(6.2)	(3.3)	(1.6)	(1.9)	(9.1)	(2.4)	(4.6)
FEH[3]	78.99	114.5	210.8	263.0	373.8	454.6	496.8	587.3	695.6	779.2	819.4	880.0
	(3.4)	(6.0)	(4.4)	(4.0)	(2.7)	(6.7)	(6.8)	(2.7)	(2.7)	(12.6)	(4.1)	(8.9)
Present method	77.066	111.26	206.23	247.57	360.61	439.46	449.38	564.86	669.66	691.34	782.02	824.78
	(0.9)	(3.0)	(2.1)	(−2.1)	(−0.9)	(3.2)	(−3.4)	(−1.2)	(−1.1)	(−0.1)	(−0.6)	(2.1)

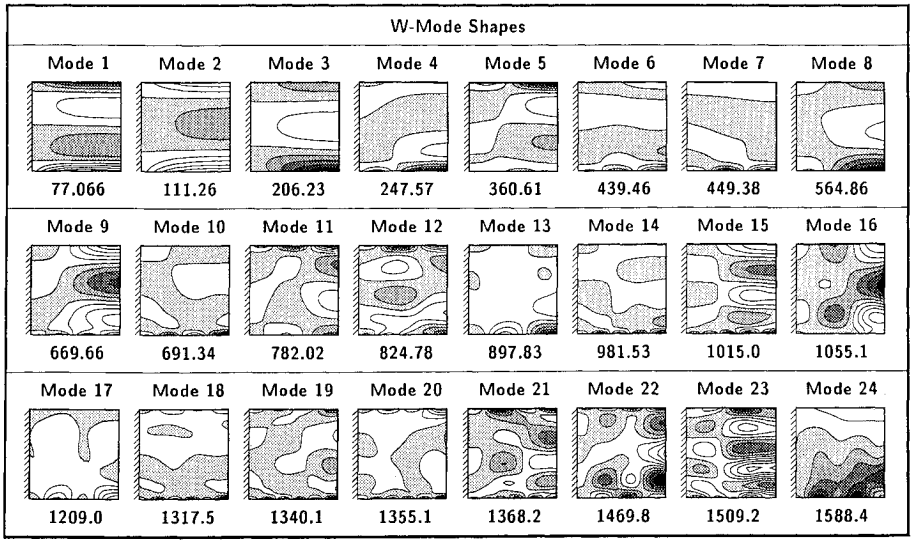

Fig. 2 Computational w-mode shapes of the CFFF cylindrical shell with y-varying thickness.

Table 2. The error percentages with reference to the experimental data are indicated in parentheses below the corresponding values.

It is observed from Table 2 that the prediction of the present *pb*-2 Ritz approach is superior to the two finite element methods with respect to the experimental natural frequencies. Particularly, the prediction of the fundamental frequency parameter of the present method has only a mere 0.9% difference as compared to 3.2% and 3.4% of FET and FEH, respectively. Besides, the error percentages of FET and FEH generally increase for higher modes of vibration. Calculations of the present *pb*-2 Ritz approach have error percentages ranging from −3.36% to 3.16%. The discrepancy in experimental and computational results is probably caused by uncertainties in Young's modulus, mass density, and tolerances in dimensions of the test specimen. On the other hand, the computational vibration nodal lines shown in Fig. 2 are closely comparable to the experimental results of Olson and Lindberg.[3] In Fig. 2 and all of the subsequent figures, shaded areas indicate regions of negative displacement amplitude whereas unshaded areas are regions of positive displacement amplitude. The lines of demarcation of the regions are the nodal lines of vibration.

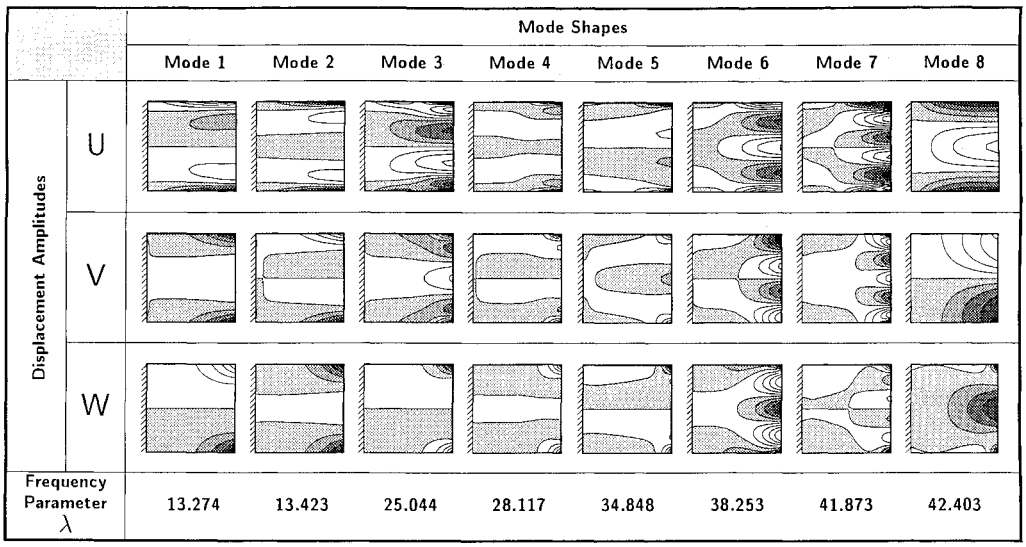

Fig. 3 In-plane and transverse vibration mode shapes of the CFFF cylindrical shell with $\nu = 0.3$, $a/b = 1.0$, $b/h_0 = 100$, $b/R_y = 0.5$, $\alpha_x = 0.00$, and $\alpha_y = 1.00$.

Table 3 Frequency parameters $\lambda = \omega ab\sqrt{\rho h_0/D_0}$ for the CFFF shallow shells with x-varying thickness

$\nu = 0.3$, $a/b = 1.0$, $b/h_0 = 100$, $\alpha_y = 1.0$

		Mode sequence number							
b/R_y	α_x	1	2	3	4	5	6	7	8
	0.00	5.2406	7.2352	12.195	15.067	16.689	18.731	22.974	25.298
	0.25	4.1136	6.9057	14.674	16.341	19.391	29.440	30.934	38.358
0.0	0.50	3.7684	7.4332	17.407	19.685	23.406	39.355	41.712	46.826
	0.75	3.5867	7.9860	19.474	23.422	27.257	47.020	53.277	54.321
	1.00	3.4712	8.5074	21.286	27.199	30.959	54.191	61.257	64.142
	0.00	7.9114	8.5522	14.048	19.079	20.642	21.152	26.343	29.900
	0.25	6.8280	7.1793	15.659	20.942	21.864	29.593	33.930	43.786
0.1	0.50	6.0270	7.5847	19.165	23.563	24.397	41.129	41.787	51.520
	0.75	5.5414	8.1019	22.393	25.501	27.993	48.261	53.370	58.489
	1.00	5.2141	8.6097	24.767	28.226	31.551	55.140	64.297	65.029
	0.00	9.1450	10.995	19.192	20.412	24.482	25.909	29.120	34.962
	0.25	7.8790	10.253	17.721	24.378	26.870	30.027	45.330	49.431
0.2	0.50	8.0185	9.5914	20.215	26.985	30.569	41.956	48.587	58.690
	0.75	8.4351	8.9063	23.480	30.027	33.183	53.239	53.560	66.915
	1.00	8.3623	8.9019	26.822	33.233	35.102	58.711	64.603	73.823
	0.00	10.543	12.036	21.817	24.688	27.923	30.048	32.226	37.143
	0.25	8.8409	12.053	21.858	27.845	29.209	30.976	49.981	53.575
0.3	0.50	8.6839	12.522	22.222	30.423	33.906	42.163	61.966	64.289
	0.75	8.9526	12.156	24.633	32.960	38.240	53.761	63.733	71.993
	1.00	9.3506	11.598	27.710	35.763	41.706	64.895	66.646	79.353
	0.00	11.953	12.771	23.354	26.795	32.861	34.803	35.303	39.488
	0.25	9.9538	12.882	27.110	29.798	31.186	33.209	50.524	57.262
0.4	0.50	9.5207	14.308	25.516	34.089	35.873	42.408	69.449	69.624
	0.75	9.6169	14.781	26.512	36.366	40.846	53.968	77.176	77.610
	1.00	9.9218	14.543	28.908	38.846	45.412	65.165	78.490	84.548
	0.00	13.274	13.423	25.044	28.117	34.848	38.253	41.873	42.403
	0.25	11.137	13.410	30.788	32.371	33.457	35.915	51.078	61.259
0.5	0.50	10.474	15.280	29.674	37.583	37.587	42.701	72.960	73.930
	0.75	10.393	16.592	29.244	39.894	42.666	54.195	82.688	82.957
	1.00	10.588	16.978	30.640	42.205	47.662	65.439	89.715	89.939

Table 4 Frequency parameters $\lambda = \omega ab\sqrt{\rho h_0/D_0}$ for the CFFF shallow shells with x-varying thickness

$\nu = 0.3$, $a/b = 5.0$, $b/h_0 = 100$, $\alpha_y = 1.0$

		Mode sequence number							
b/R_y	α_x	1	2	3	4	5	6	7	8
	0.00	1.0225	2.9349	5.0559	5.8238	7.8024	9.6907	11.859	12.024
	0.25	0.80390	3.1217	5.7827	7.5025	12.079	14.030	19.892	22.738
0.0	0.50	0.73705	3.5345	6.2212	9.1442	15.366	17.560	25.963	28.825
	0.75	0.70188	3.9092	6.5329	10.595	18.179	20.639	31.150	34.096
	1.00	0.67954	4.2536	6.7835	11.935	20.749	23.469	35.868	38.928
	0.00	2.0792	5.4309	8.0816	9.6301	13.490	15.875	20.026	21.561
	0.25	1.5162	5.7981	6.8904	12.252	16.852	20.640	29.930	30.887
0.1	0.50	1.2967	6.2360	6.6837	15.475	17.150	26.362	31.420	39.016
	0.75	1.1759	6.5501	6.6764	17.693	18.281	31.481	32.937	46.516
	1.00	1.0985	6.7533	6.8035	18.372	20.854	34.607	36.178	53.472
	0.00	3.6619	5.7118	11.104	12.992	17.554	18.880	25.096	27.692
	0.25	2.6559	5.8398	12.311	12.720	22.470	28.958	34.975	39.837
0.2	0.50	2.2429	6.2771	11.723	15.779	27.495	29.566	41.744	51.824
	0.75	2.0077	6.5991	11.435	18.576	29.789	32.433	48.706	53.525
	1.00	1.8524	6.8604	11.283	21.156	30.089	37.074	54.814	55.431
	0.00	5.3066	5.9555	12.491	15.229	21.434	23.826	28.685	30.196
	0.25	3.8574	5.9039	13.407	17.750	24.917	36.560	40.105	43.615
0.3	0.50	3.2496	6.3389	16.248	16.966	29.243	41.624	45.796	65.207
	0.75	2.8998	6.6734	16.484	19.028	33.920	42.160	52.099	71.027
	1.00	2.6669	6.9463	16.169	21.621	38.469	42.454	58.483	65.228
	0.00	6.1914	6.9368	13.895	16.619	23.658	29.243	32.486	33.131
	0.25	5.0673	5.9883	14.266	22.852	27.768	38.885	45.785	48.236
0.4	0.50	4.2674	6.4162	16.858	22.154	31.487	50.772	51.964	65.554
	0.75	3.8041	6.7663	19.605	21.542	35.847	53.706	56.434	71.032
	1.00	3.4945	7.0532	21.104	22.212	40.268	54.364	62.408	65.237
	0.00	6.4328	8.5219	15.339	17.773	25.625	32.284	36.489	37.897
	0.25	6.0915	6.2692	15.265	27.297	30.898	40.594	50.747	51.707
0.5	0.50	5.2822	6.5056	17.592	27.181	34.118	56.354	59.557	66.169
	0.75	4.7071	6.8723	20.281	26.516	38.137	61.468	63.796	71.039
	1.00	4.3217	7.1748	22.897	25.991	42.390	65.210	65.270	67.055

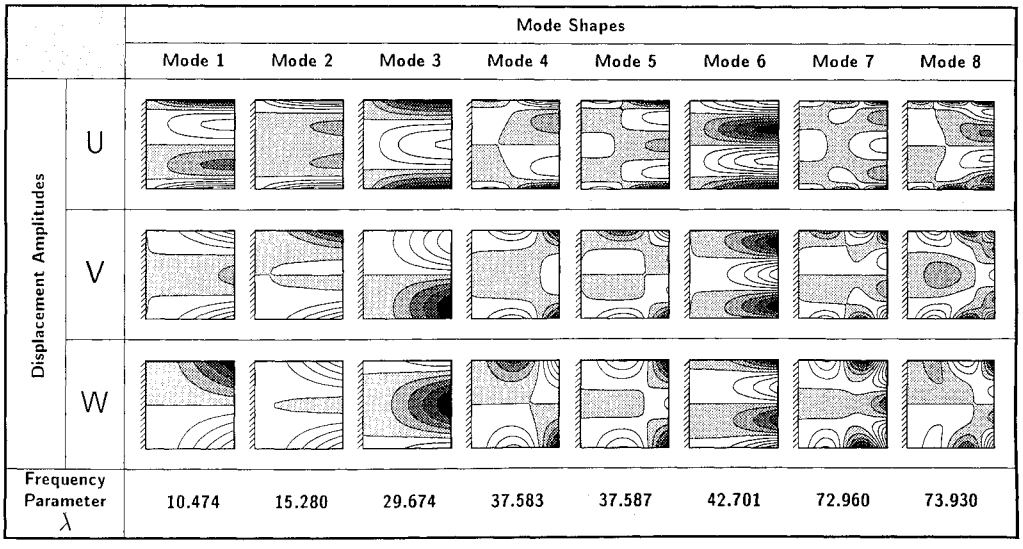

Fig. 4 In-plane and transverse vibration mode shapes of the CFFF cylindrical shell with $\nu = 0.3$, $a/b = 1.0$, $b/h_0 = 100$, $b/R_y = 0.5$, $\alpha_x = 0.50$, and $\alpha_y = 1.00$.

The order of mode shape arrangement in Fig. 2 is somewhat different from the arrangement of Olson and Lindberg[3] by ascending calculated frequencies. If we go by the order of ascending experimental frequencies, modes 14, 15, 16, and 17 of Olson and Lindberg[3] should be reassigned as modes 15, 16, 14, and 17 correspondingly. This new arrangement is exactly parallel to the present arrangement, as shown in Fig. 2. The fact that the FET method predicts an ambiguous order of mode shape arrangement further authenticates the inaccuracy of the result for higher modes of vibration of a shallow shell. This fact has also been observed and discussed in detail by Lim and Liew[14] recently in dealing with the vibration of a fan blade with uniform thickness.

The present shallow shell model can also be used to simulate a flat plate by assigning an infinite radius of curvature $R_y \to \infty$. The formulation presented in Sec. II reduces to variable thickness flat plate equations of Liew and Lim.[13] A comparison of results using flat plate equations and the present formulation

($R_y \to \infty$) has been performed, and the eigenvalues are in excellent agreement.

C. Numerical Results and Mode Shapes

Results of the nondimensional frequency parameters $\lambda = \omega ab\sqrt{\rho h_0/D_0}$ are tabulated in Tables 3–6. The thickness variation ratios α_x and α_y are not varied simultaneously where either one is assigned 1.0 (uniform thickness) at a time. Tables 3 and 4 present the results of x-varying thickness with $\alpha_x = 0.00$, 0.25, 0.50, 0.75, and 1.00, and Tables 5 and 6 present the results of y-varying thickness with $\alpha_y = 0.0$, 0.5, 1.0, 1.5, and 2.0. The aspect ratios (a/b) investigated are 1.0 and 5.0 which cover wide spectrum of shallowness ratio (b/R_y) ranging from 0.0 (flat plate) to 0.5.

The effects of thickness variation ratios α_x and α_y, which constitute the key subject of the present paper, are extensively studied and displayed in Tables 3–6. It is observed, generally, that increases in the ratios result in higher values of λ. Since λ is directly proportional to the physical frequencies of vibration ω, it can be deduced that higher thickness variation ratios are

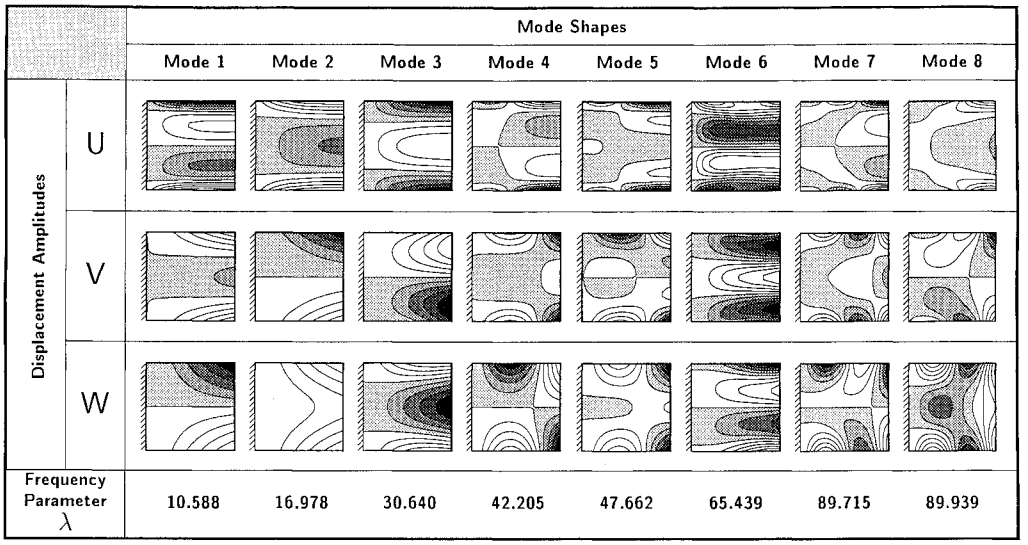

Fig. 5 In-plane and transverse vibration mode shapes of the CFFF cylindrical shell with $\nu = 0.3$, $a/b = 1.0$, $b/h_0 = 100$, $b/R_y = 0.5$, $\alpha_x = 1.00$, and $\alpha_y = 1.00$.

Table 5 Frequency parameters $\lambda = \omega ab\sqrt{\rho h_0/D_0}$ for the CFFF shallow shells with y-varying thickness

$\nu = 0.3$, $a/b = 1.0$, $b/h_0 = 100$, $\alpha_x = 1.0$

		Mode sequence number							
b/R_y	α_y	1	2	3	4	5	6	7	8
0.0	0.0	2.3790	5.7188	10.478	14.667	16.198	17.740	23.378	25.396
	0.5	2.7128	6.4925	15.685	20.253	23.350	39.067	41.309	47.801
	1.0	3.4712	8.5074	21.286	27.199	30.959	54.191	61.257	64.142
	1.5	4.4048	10.697	26.439	33.904	38.783	67.105	72.519	80.311
	2.0	5.4257	12.985	31.370	40.506	46.700	78.135	82.617	95.602
0.1	0.0	3.9161	6.1244	12.828	14.849	19.108	20.670	25.224	26.263
	0.5	4.6868	6.6835	19.101	21.233	25.169	40.771	43.869	47.991
	1.0	5.2141	8.6097	24.767	28.226	31.551	55.140	64.297	65.029
	1.5	5.8745	10.798	29.447	34.435	39.452	67.883	74.777	80.534
	2.0	6.6598	13.099	33.835	40.806	47.467	79.116	83.928	95.695
0.2	0.0	6.0777	7.0325	14.901	15.620	22.236	26.757	28.574	29.353
	0.5	7.0752	7.8895	20.447	24.442	31.332	45.953	47.804	49.828
	1.0	8.3623	8.9019	26.822	33.233	35.102	58.711	64.603	73.823
	1.5	8.8249	11.057	32.874	37.934	42.325	70.446	79.117	82.017
	2.0	9.3622	13.363	38.185	42.446	50.310	81.516	87.714	95.962
0.3	0.0	6.8392	9.2688	15.875	17.358	24.779	28.719	30.550	31.598
	0.5	7.6232	10.893	21.573	27.322	35.577	48.105	53.189	58.461
	1.0	9.3506	11.598	27.710	35.763	41.706	64.895	66.646	79.353
	1.5	11.435	12.068	33.874	41.369	48.761	75.822	80.337	87.049
	2.0	12.501	13.718	39.931	45.822	56.086	85.475	92.523	96.600
0.4	0.0	7.4620	11.112	17.354	18.955	26.898	29.230	33.529	34.148
	0.5	8.2911	13.258	23.384	30.151	38.246	48.455	57.553	70.164
	1.0	9.9218	14.543	28.908	38.846	45.412	65.165	78.490	84.548
	1.5	11.922	15.222	34.790	44.237	54.249	80.643	84.863	92.527
	2.0	14.133	15.709	40.822	48.826	62.539	91.721	95.510	99.549
0.5	0.0	8.1412	12.216	19.456	20.429	28.717	29.560	36.373	36.781
	0.5	9.0505	14.842	25.984	32.712	40.679	48.854	61.270	74.749
	1.0	10.588	16.978	30.640	42.205	47.662	65.439	89.715	89.939
	1.5	12.496	18.105	35.985	47.240	57.791	80.947	94.829	99.532
	2.0	14.638	18.774	41.758	51.670	67.462	95.593	100.24	105.85

Table 6 Frequency parameters $\lambda = \omega ab\sqrt{\rho h_0/D_0}$ for the CFFF shallow shells with y-varying thickness

$\nu = 0.3$, $a/b = 5.0$, $b/h_0 = 100$, $\alpha_x = 1.0$

		Mode sequence number							
b/R_y	α_y	1	2	3	4	5	6	7	8
	0.0	0.47788	2.9575	5.7369	8.1199	15.355	16.742	23.959	26.688
	0.5	0.53643	3.3372	5.4417	9.2806	16.459	18.009	27.973	29.426
0.0	1.0	0.67954	4.2536	6.7835	11.935	20.749	23.469	35.868	38.928
	1.5	0.86573	5.4052	8.6918	15.113	26.473	29.566	45.482	48.759
	2.0	1.0729	6.6743	10.883	18.561	32.918	36.018	55.946	58.852
	0.0	0.82270	5.0705	5.8031	13.818	17.042	25.805	27.484	36.460
	0.5	1.0051	5.4709	6.1599	16.446	16.796	28.298	30.957	41.317
0.1	1.0	1.0985	6.7533	6.8035	18.372	20.854	34.607	36.178	53.472
	1.5	1.2192	7.5143	8.7129	20.552	26.571	38.944	45.797	61.730
	2.0	1.3687	8.4455	10.906	23.149	33.022	43.936	56.313	64.077
	0.0	1.4165	5.8842	8.6506	17.553	22.905	29.281	38.861	43.107
	0.5	1.7786	5.5511	10.800	17.043	28.411	29.804	43.889	51.197
0.2	1.0	1.8524	6.8604	11.283	21.156	30.089	37.074	54.814	55.431
	1.5	1.9203	8.7564	11.732	26.809	31.511	46.440	58.065	64.815
	2.0	2.0077	10.938	12.305	32.866	33.566	56.578	61.843	64.079
	0.0	2.0429	6.0040	12.164	18.536	28.072	35.592	42.359	53.763
	0.5	2.5905	5.6604	15.466	17.836	31.167	40.723	47.642	64.063
0.3	1.0	2.6669	6.9463	16.169	21.621	38.469	42.454	58.483	65.228
	1.5	2.7069	8.8291	16.457	27.209	43.643	47.645	64.816	71.128
	2.0	2.7563	11.008	16.804	33.575	44.909	57.789	64.082	81.534
	0.0	2.6643	6.1576	14.970	20.357	30.409	44.126	46.468	53.770
	0.5	3.4030	5.7960	17.880	20.986	33.289	51.477	52.279	64.068
0.4	1.0	3.4945	7.0532	21.104	22.212	40.268	54.364	62.408	65.237
	1.5	3.5165	8.9210	21.286	27.741	49.040	55.947	64.819	74.465
	2.0	3.5401	11.088	21.496	34.043	56.591	59.497	64.086	87.674
	0.0	3.2649	6.3472	16.730	23.255	32.618	51.037	51.299	53.781
	0.5	4.2000	5.9575	18.787	25.629	35.731	57.507	60.346	64.075
0.5	1.0	4.3217	7.1748	22.897	25.991	42.390	65.210	65.270	67.055
	1.5	4.3299	9.0283	25.970	28.510	50.855	64.825	67.642	78.421
	2.0	4.3337	11.183	26.180	34.651	60.338	64.093	69.233	91.119

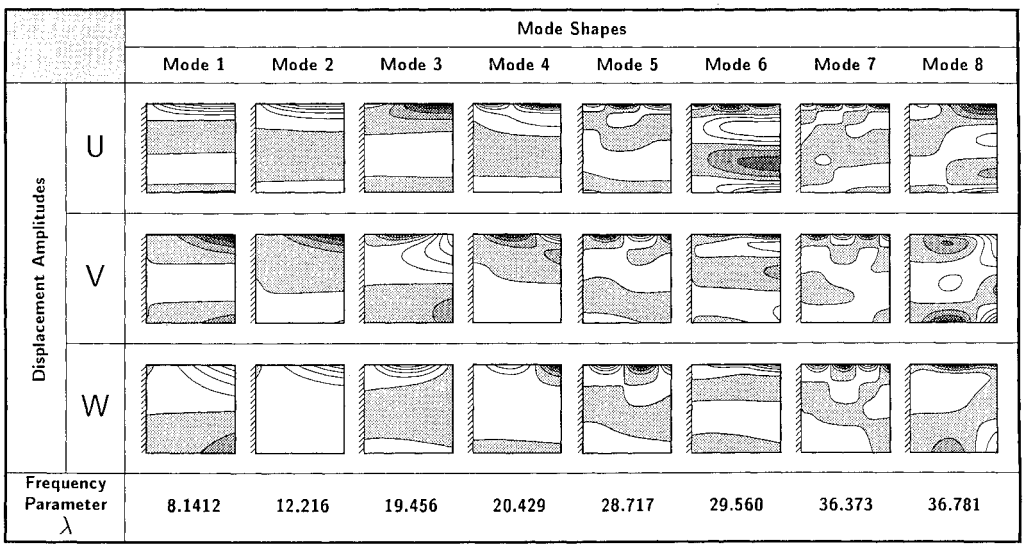

Fig. 6 In-plane and transverse vibration mode shapes of the CFFF cylindrical shell with $\nu = 0.3$, $a/b = 1.0$, $b/h_0 = 100$, $b/R_y = 0.5$, $\alpha_x = 1.00$, and $\alpha_y = 0.00$.

associated with higher physical frequency of vibration and, hence, higher shell structural stiffness. However, for certain lower modes with $\alpha_y = 1.0$ in Tables 3 and 4, λ decreases and may reach a minimum value before it magnifies subsequently.

Moreover, the results in Tables 3–6 also illustrate that a deeper shell (higher value of b/R_y) has higher values of λ and, consequently, higher values of the physical frequency ω, assuming b remains constant. Therefore, the shell structural stiffness increases for a deeper shallow shell.

A set of the in-plane and transverse vibration mode shapes for different thickness variation ratios are given in Figs. 3-7. The selected shells have specifications $\nu = 0.3$, $a/b = 1.0$, $b/h_0 = 100$, and $b/R_y = 0.5$. Shaded regions possesses negative displacement amplitude whereas unshaded regions do not. The lines of demarcation in between shaded and unshaded regions are the nodal lines of vibration. For $\alpha_y = 1.0$, the modes are either x symmetric or x antisymmetric. However, no symmetry is observed for $\alpha_x = 1.0$ and $\alpha_y \neq 1.0$. Further-

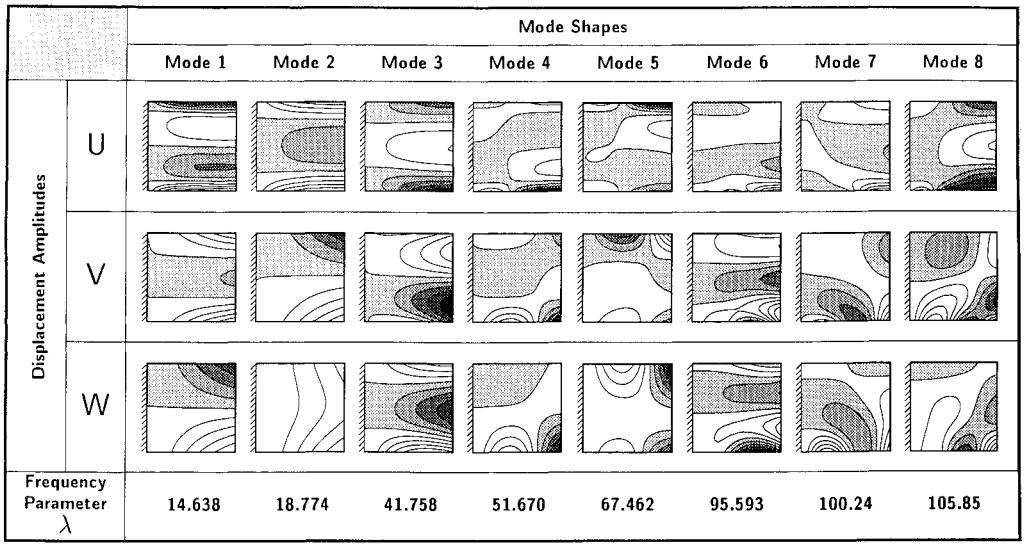

Fig. 7 In-plane and transverse vibration mode shapes of the CFFF cylindrical shell with $\nu = 0.3$, $a/b = 1.0$, $b/h_0 = 100$, $b/R_y = 0.5$, $\alpha_x = 1.00$, and $\alpha_y = 2.00$.

more, contour lines are comparatively more densely distributed for those regions with very thin thickness indicating abrupt changes in in-plane and transverse displacement amplitude. The higher modes have more nodal lines and are more complex in nature.

IV. Conclusions

A computational model based on the *pb*-2 Ritz energy approach is developed to simulate the vibratory response of variable thickness cantilevered shallow cylindrical shell of rectangular planform. This method is relatively simpler, highly versatile, more accurate, and less costly in computational preparation and implementation as compared to the other numerical approaches. The global *pb*-2 shape function, which is formed from the product of a set of mathematically complete two-dimensional polynomials and a basic function, satisfies the geometric boundary conditions of the cantilevered shallow shell explicitly. A linear two-dimensional thickness variation function is also introduced in the formulation to simulate the shells of nonuniform thickness.

Numerical convergence of the eigenvalues is established as the degree of polynomial increases, as shown in Table 1. Comparison with experimental and finite element results is presented in Table 2, which reveals a better and superior *pb*-2 Ritz approach over the finite element method with respect to the experimental data. Incorrect mode shape arrangement using the finite element method is also discussed at length. The present method can also be used to simulate a flat plate by assigning $R_y \to \infty$.

Extensive numerical results are presented in Tables 3-6 for wide ranges of shell aspect ratio, shallowness ratio, and thickness variation ratios. It is noted that the shell structural stiffness is greatly dependent on the increases in thickness variation ratios. It is also found that a deeper shallow shell exhibits higher physical frequencies and, hence, higher structural stiffness. A set of vibration mode shapes for different thickness variation ratios is presented in Figs. 3-7.

References

[1]Leissa, A. W., "Vibration of Shells," NASA SP-288, 1973.

[2]Lee, J. K., Leissa, A. W., and Wang, A. J., "Vibrations of Blades with Variable Thickness and Curvature by Shell Theory," *Journal of Engineering for Gas Turbines and Power,* Vol. 106, Jan. 1984, pp. 11-16.

[3]Olson, M. D., and Lindberg, G. M., "Dynamic Analysis of Shallow Shell with a Doubly-Curved Triangular Finite Element," *Journal of Sound and Vibration,* Vol. 19, No. 3, 1971, pp. 299-318.

[4]Walker, K. P., "Vibrations of Cambered Helicoidal Fan Blades," *Journal of Sound and Vibration,* Vol. 59, No. 1, 1978, pp. 35-57.

[5]Deb Nath, J. M., "Dynamics of rectangular curved plates," Ph.D. Thesis, Univ. of Southampton, Southampton, England, UK, 1969.

[6]Petyt, M., "Vibration of Curved Plates," *Journal of Sound and Vibration,* Vol. 15, No. 3, 1971, pp. 381-395.

[7]Leissa, A. W., Lee, J. K., and Wang, A. J., "Vibrations of Cantilevered Shallow Cylindrical Shells of Rectangular Planform," *Journal of Sound and Vibration,* Vol. 78, No. 3, 1981, pp. 311-328.

[8]Leissa, A. W., Lee, J. K., and Wang, A. J., "Rotating Blade Vibration Analysis Using Shells," *Journal of Engineering for Power,* Vol. 104, April 1982, pp. 296-302.

[9]Leissa, A. W., and Ewing, M. S., "Comparison of Beam and Shell Theories for the Vibrations of Thin Turbomachinery Blades," *Journal of Engineering for Power,* Vol. 105, April 1983, pp. 383-392.

[10]Cheung, Y. K., Li, W. Y., and Tham, L. G., "Free Vibration Analysis of Singly Curved Shell by Spline Finite Strip Method," *Journal of Sound and Vibration,* Vol. 128, No. 3, 1989, pp. 411-422.

[11]Liew, K. M., and Wang, C. M., "*pb*-2 Rayleigh-Ritz Method for General Plate Analysis," *Engineering Structures,* Vol. 15, 1993, pp. 55-60.

[12]Liew, K. M., "Response of Plates of Arbitrary Shape Subject to Static Loading," *Journal of Engineering Mechanics,* Vol. 118, No. 9, 1992, pp. 1783-1794.

[13]Liew, K. M., and Lim, M. K., "Transverse Vibration of Trapezoidal Plates of Variable Thickness: Symmetric Trapezoids," *Journal of Sound and Vibration,* Vol. 165, No. 1, 1993, pp. 329-340.

[14]Lim, C. W., and Liew, K. M., "A *pb*-2 Ritz Formulation for Flexural Vibration of Shallow Cylindrical Shells of Rectangular Planform," *Journal of Sound and Vibration* (to be published).